ChemPubSoc Europe

DOI: 10.1002/cssc.201700500

CHEMSUSCHEM Full Papers

Freestanding Gold/Graphene-Oxide/Manganese Oxide Microsupercapacitor Displaying High Areal Energy Density

Ahiud Morag,[a, b] James Y. Becker,[a] and Raz Jelinek*[a, b]

Microsupercapacitors are touted as one of the promising "next frontiers" in energy-storage research and applications. Despite their potential, significant challenges still exist in terms of physical properties and electrochemical performance, particularly attaining high energy density, stability, ease of synthesis, and feasibility of large-scale production. We present new freestanding microporous electrodes comprising self-assembled scaffold of gold and reduced graphene oxide (rGO) nanowires coated with MnO_2. The electrodes exhibited excellent electrochemical characteristics, particularly superior high areal capacitance. Moreover, the freestanding Au/rGO scaffold also served as the current collector, obviating the need for an additional electrode support required in most reported supercapacitors, thus enabling low volume and weight devices with a high overall device specific energy. Stacked symmetrical solid-state supercapacitors were fabricated using the Au/rGO/MnO_2 electrodes in parallel configurations showing the advantage of using freestanding electrodes in the fabrication of low-volume devices.

Introduction

The search for innovative energy-storage devices in microelectronics applications and devices has considerably expanded over the last few years.[1–9] Most energy-storage devices in microelectronics today are based on batteries. The fundamental drawbacks of microbatteries, however, are the low power density, low energy retention, and safety issues.[10,11] Microsupercapacitors have emerged as promising substituents of traditional microbatteries as they exhibit high power densities and efficient capacitance retention.[1,6,12] Two technologies have been mainly pursued in supercapacitor research, specifically electrical double-layer capacitors (EDLCs), and pseudocapacitors.[1,3,13–15] Although EDLCs exhibit high power densities, their low energy densities constitute a major impediment for their energy-storage application in microelectronics. Pseudocapacitors, usually based on transition metal oxides that store energy through fast and reversible faradaic redox reactions, have shown great potential owing to their high energy-storage capabilities compared to EDLCs.[8,16] A significant drawback in many reported pseudocapacitors is that despite of the high capacitance reported, the latter has been generally normalized to either the weight or the volume of the active material.[17–21] Although these values underscore high overall capacitance, the specific capacitances of many such devices, which include also the weight/volume of the complete device (primarily the electrode scaffolding that serves as the current collector), are low and not suitable for commercial uses. Furthermore, there is generally no linear relationship between the volume/weight of the active material and device performance, limiting applicability of pseudocapacitor technology for practical energy-storage applications.[17,18,21] Varied freestanding carbon-based electrodes and supercapacitors have been reported in recent years, however, the energy density of such device has generally been low.[22–25] Accordingly, enhancing the areal capacitance, a more pertinent parameter for energy-storage capabilities, has become a critical strategy for advancing microsupercapacitor technologies. Recent studies reported varied strategies for construction of pseudocapacitor-based devices exhibiting high areal capacitance.[26–30]

Here, we present a new freestanding composite electrode consisting of gold/reduced graphene oxide (rGO) porous matrix coated with pseudocapacitive MnO_2, which exhibits superior electrochemical performance and overcomes many of the above-mentioned limitations for microsupercapacitor applications. The Au/rGO/MnO_2 electrode was fabricated through a simple solution-based method consisting of self-assembly of highly porous Au/rGO scaffold followed by electrodeposition of MnO_2. The electrode displayed excellent electrochemical properties, particularly very high areal capacitance. A symmetric solid-state microsupercapacitor comprising Au/rGO/MnO_2 electrodes was assembled, exhibiting high areal energy density and making the new electrode technology a promising conduit for energy-storage applications in microelectronics.

[a] A. Morag, Prof. Dr. J. Y. Becker, Prof. Dr. R. Jelinek
Department of Chemistry
Ben-Gurion University of the Negev
Beer-Sheva 8410501 (Israel)
E-mail: razj@bgu.ac.il

[b] A. Morag, Prof. Dr. R. Jelinek
Ilse Katz Institute for Nanoscale Science and Technology
Ben-Gurion University of the Negev
Beer-Sheva 8410501 (Israel)

Supporting Information and the ORCID identification number(s) for the author(s) of this article can be found under: https://doi.org/10.1002/cssc.201700500.

Results and Discussion

Electrode characterization

Scheme 1 illustrates Au/rGO/MnO_2 electrode fabrication. The assembly of the Au scaffold was based upon a recently reported simple chemical process in which $KAu(SCN)_4$ (prepared by mixing chloroauric acid and potassium thiocyanate), is self-reduced into metallic Au nanostructures without coaddition of reducing agents.[31,32] As depicted in Scheme 1, the initial step consisted of mixing $KAu(SCN)_4$ and GO in water/acetonitrile and slowly drying the suspension upon a glass surface. The porous microwire network formed was subjected to air plasma, which was previously shown to aid complete reduction of the Au framework,[31] and reaction with hydrazine designed to generate the conductive metallic Au/rGO framework. In a final step, electrodeposition of MnO_2 was performed yielding the freestanding Au/rGO/MnO_2 electrode (Scheme 1, right).

Scanning electron microscopy (SEM) analysis was done to assess the electrode morphology (Figure 1). The SEM images of the Au/rGO matrix prior to MnO_2 deposition in Figures 1 A–C show a highly porous microwire network. Close inspection of the surfaces of the Au/rGO wires reveal a sponge-like morphology featuring abundant nanopores (Figure 1 C). Importantly, the incorporation of rGO within the Au framework was found to enhance mechanical stability of the microwires and overall resilience of the composite structure. X-ray photoelectrons spectroscopy (XPS) (Figure S1 in the Supporting Information), Raman spectroscopy (Figure S2), and X-ray diffraction (XRD, Figure S3) analyses confirm that the microwires depicted in Figure 1 A–C consist of both metallic Au and rGO following air plasma and hydrazine treatments.

The SEM images of the Au/rGO microwire framework after MnO_2 electrodeposition indicate effective coating of the microwires with the pseudocapacitive MnO_2 (Figure 1 D–F). Cross-section microscopy experiments confirmed MnO_2 deposition also within the internal core of the Au/rGO microwire layer (Figure S4). Electrochemical analysis, measured for deposition time between 4–16 min, indicates optimal MnO_2 electrodeposition time of 12 min. Although the specific capacitance is known to decrease with thicker coating,[33] 12 min-MnO_2 deposition produced in our case the highest areal capacitance (Figure S5). XPS analysis of the Mn 2p peaks confirmed that electrodeposition indeed yielded a MnO_2 layer (Figure S6). In particular, the SEM data in Figure 1 D–F demonstrate that MnO_2 deposition did not adversely affect the microwire scaffold organization, and the nanoporous surface area was retained. Overall, the microscopic characterization in Figure 1 attests to the highly porous organization and extensive surface area of the Au/rGO/MnO_2 electrode, which constitute critical parameters for its electrochemical performance, as these structural features enable unhindered ion diffusion and efficient charge transfer processes.[2,34–38]

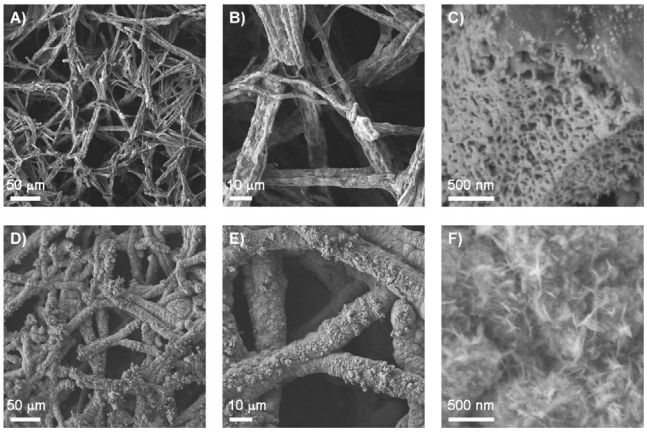

Figure 1. Morphology of Au/rGO/MnO_2 electrode: A–C) SEM images of the Au/rGO electrode (before MnO_2 deposition) at different magnifications. The darker domains apparent on the surfaces of the wires in B) and C) correspond to rGO, whereas the brighter areas are ascribed to metallic Au. D–F) SEM images of the Au/rGO electrode after electrodeposition of MnO_2.

Electrochemical performance

Electrochemical characterization of the Au/rGO/MnO_2 electrode was done by cyclic voltammetry (CV) and galvanostatic measurements (Figure 2) using a three-electrode cell configuration in 1 M LiCl solution as electrolyte. Figure 2 A depicts the CV curves for scan rates ranging from 1 to 100 mV s^{-1}. The symmetrical semirectangular shapes of the curves confirm the pseudocapacitive behavior of the electrode,[1,39] as well as its low resistivity indicating effective ion diffusion and charge transfer at the electrode interface.[40,41] CV analysis of the Au/rGO electrode without MnO_2 electrodeposition (Figure S7) showed an order-of-magnitude lower capacitance than that shown in Figure 2 A, confirming that the pronounced capacitance of the Au/rGO/MnO_2 electrode arises from the MnO_2 layer. This capacitance is much higher than the capacitance achieved using only Au scaffold.[31] Figure 2 B depicts specific areal capacitance values at different scan rates, calculated from

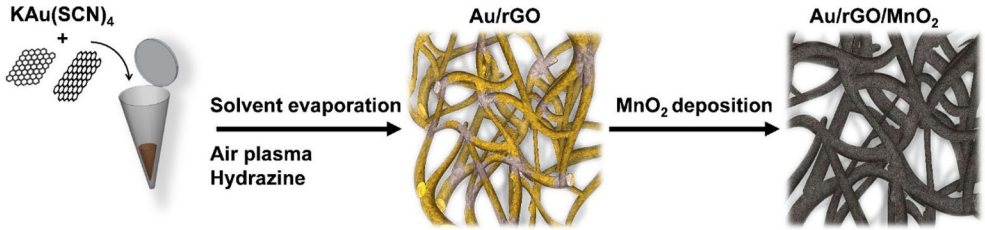

Scheme 1. Fabrication of Au/rGO/MnO_2 electrode. The porous microwire scaffold (middle) is comprised of rGO (grey) interspersed with Au (yellow). The microwire scaffold is subsequently coated uniformly with MnO_2 (shown in black, right).

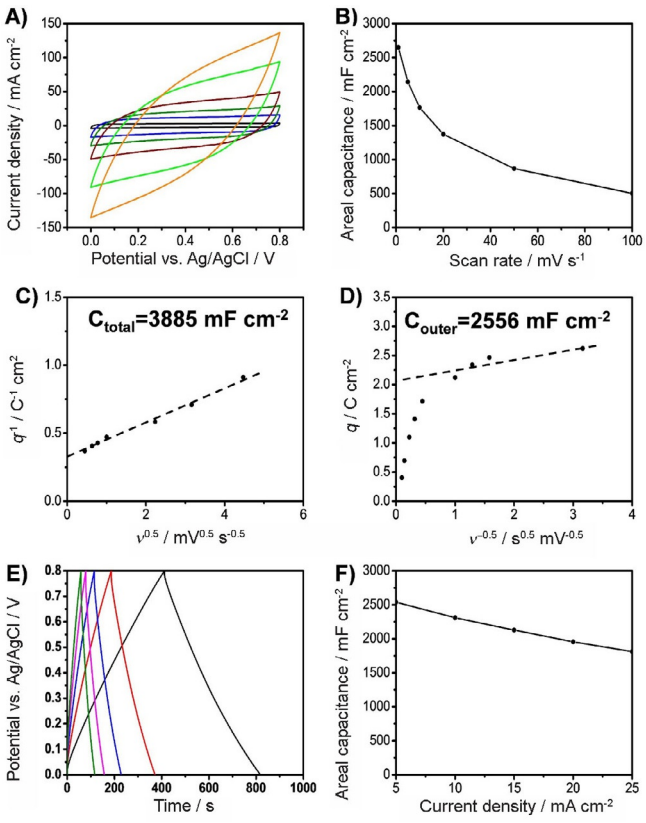

Figure 2. Electrochemical characterization of the Au/rGO/MnO_2 electrode: A) CV curves at scan rates of 1, 5, 10, 20, 50, and 100 mV s^{-1} in 1 M LiCl. B) Calculated areal capacitance as a function of scan rate. C) Reverse areal voltammetric charge as a function of the square root of the scan rate. The dashed line corresponds to the linear fitting of the data. D) Areal voltammetric charge as a function of reverse square root of the scan rate. The dashed line corresponds to the linear fitting of scan rate between 0.1 to 1.0 mV s^{-1}. E) Galvanostatic charge/discharge at current densities of 5, 10, 15, 20, and 25 mA cm^{-2} in 1 M LiCl. F) Calculated areal capacitance as a function of the current density.

the CV curves shown in Figure 2A. The significant areal capacitance of the Au/rGO/MnO_2 electrode is higher than values recently reported,[27,42,43] and highlights the effective utilization of the electrode surface area for efficient charge transfer.

The total and outer areal capacitance outlined in Figure 2C–D further attest to the ion accessibility and charge transfer upon the electrode surface.[16,28,44] Specifically, the total area capacitance, extrapolated from the curve of q^{-1} (inverse areal voltammetric charge) as a function of the square root of scan rate (v) (Figure 2C), was almost 4000 mF cm^{-2}, which is higher than recently published values.[28,44] Notably, the outer surface areal capacitance of the Au/rGO/MnO_2 electrode was 2556 mF cm^{-2}, obtained from extrapolating the curve of q versus $v^{-0.5}$ to $v^{-0.5}=0$ (Figure 2D), is significant, emphasizing the potential utilization of the electrode in supercapacitor applications. The calculated ratio between the outer surface and total area capacitance of the Au/rGO/MnO_2 electrode is 66%, which is among the highest values published so far,[45–48] similarly indicates suitability for energy-storage devices.

Additional measurements attest to the superior electrochemical performance of the Au/rGO/MnO_2 electrode. Galvanostatic charge/discharge (GCD) curves were recorded to characterize the electrode response at constant currents (Figure 2E). The almost linear and symmetrical appearances of the GCD curves at current densities ranging from 5 to 25 mA cm^{-2} indicate that the electrode facilitates reversible redox reactions and its performance is close to ideal supercapacitance.[49,50] In particular, the high capacitance was retained even at a high current density of 25 mA cm^{-2}, exhibiting a long (58 s) discharge time (Figure 2E). The specific areal capacitance calculated from the GCD curves is presented in Figure 2F, further displaying the excellent capacitance properties of the electrode even at high current densities. Specifically, the capacitance of 2540 mF cm^{-2} recorded at a current density of 5 mA cm^{-2} is higher than the corresponding values obtained for previously reported electrodes[27,29] (a detailed comparison between the properties of the Au/rGO/MnO_2 electrode and previously reported electrodes is provided in Table S1). Figure 2F indicates a high (71%) areal capacitance retention when the current density was increased from 5 to 25 mA cm^{-2}, consistent with high conductivity and good electrolyte diffusion. Indeed, the equivalent series resistance corresponding to the Au/rGO/MnO_2 electrode (2.00 Ω cm^2) is rather small, as shown in the Nyquist plot (Figure S8), and lower than recent metal-based pseudocapacitive devices.[29,44] In addition, the near-vertical line in the low frequency region of the Nyquist plot indicates a near-ideal capacitor behavior.[11,51–53]

Solid-state supercapacitors

Figure 3 depicts utilization of the Au/rGO/MnO_2 electrodes in a symmetric solid-state microsupercapacitor. Figure 3Ai shows a scheme of the symmetric microsupercapacitor, assembled by using two Au/rGO/MnO_2 electrodes, filter paper as the spacer between the electrodes, and LiCl/polyvinyl alcohol (PVA) as the electrolyte (Figure S9 shows the assembly process of the symmetric device, and Figure S10 exhibits photos of the freestanding electrode and the solid-state device). A microsupercapacitor device comprising of two stacked electrodes in parallel is illustrated in Figure 3Ai. Figure 3B presents the GCD curves for current densities from 1.5 to 25 mA cm^{-2} recorded for the symmetric device outlined in Figure 3Ai. The near linearity and symmetrical appearance of the curves indicate that the solid-state device exhibits a near-ideal supercapacitor behavior.[49,50] Notably, the inset in Figure 3B reveals a voltage drop (*IR* drop) of 25 mV at a current density of 1.5 mA cm^{-2}, indicating an overall device resistance of 16.7 Ω cm^{-2}. This resistance value is low compared to recently published devices[28] and makes the symmetric Au/rGO/MnO_2 supercapacitor practical even at high current densities. From the voltage drop, a maximum power density of 9.58 mW cm^{-2} (269.9 mW cm^{-3}) can be calculated, comparable to previously published symmetric devices (Table S1).

Figure 3C depicts the specific areal capacitance of the symmetric two-electrode device, calculated from the GCD curves. The graph in Figure 3C indicates a capacitance of 1532 mF cm^{-2} at 1.5 mA cm^{-2}, yielding an energy density of 0.136 mWh cm^{-2}. When considering two electrodes, each with

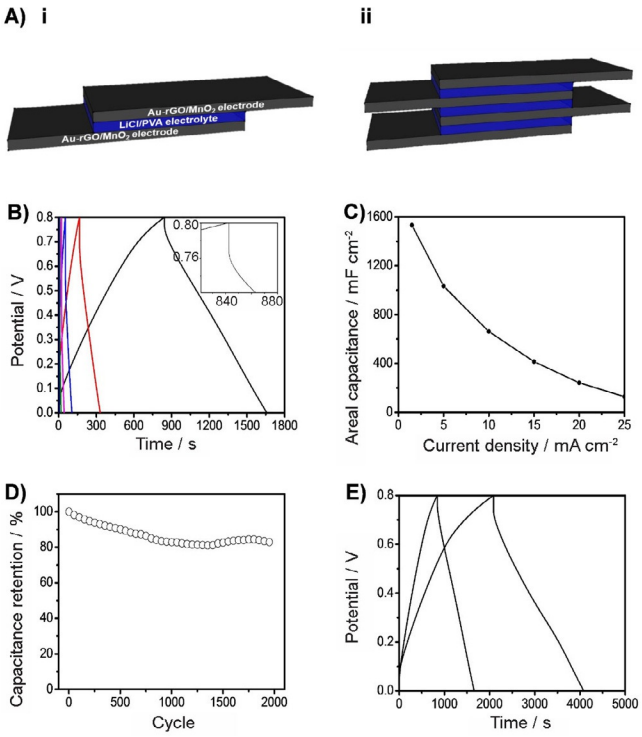

Figure 3. Electrochemical characterization of symmetric solid-state microsupercapacitors comprising Au/rGO/MnO_2 electrodes: A) Schematic of a single device (i) and a stacked device of two supercapacitors in parallel (ii). B) Galvanostate charge/discharge at current densities of 1.5, 5, 10, 15, 20, and 25 mA cm^{-2}. The inset shows the *IR* drop at a current density of 1.5 mA cm^{-2}. C) Calculated capacitance as a function of the current density. D) Capacitance retention at a current density of 15 mA cm^{-2} over 2000 cycles. E) Galvanostate charge/discharge at a current density of 1.5 mA cm^{-2} for devices assembled from one (left) and two (right) symmetric microsupercapacitors in parallel configuration.

a thickness of 130 μm, and filter paper as separator (100 μm), a volumetric energy density of 3.83 mWh cm^{-3} is calculated. This value is higher than many recently published devices (Table S1), and indicates the potential use of Au/rGO/MnO_2-based solid-state devices in energy-storage applications. The nonlinear decrease of the areal capacitance as a function of current density (Figure 3C) likely reflects ion diffusion effects; a similar phenomenon was reported in other solid-state supercapacitors.[36,37] The two-electrode microsupercapacitor exhibited excellent stability, retaining 83% of the initial capacitance after over 2000 cycles at a current density of 15 mA cm^{-2} (Figure 3D).

An important advantage of the Au/rGO/MnO_2 electrode is the fact that the Au/rGO matrix constitutes both the scaffold for the pseudocapacitive layer and the current collector. Consequently, several electrodes can be stacked to produce low-volume and low-weight parallel device configurations (device illustrated in Figure 3Aii). Figure 3E presents the GCD curves recorded at a current density of 1.5 mA cm^{-2} corresponding to a single (left GCD curve) and two-stacked microsupercapacitors (right GCD curve), comprising two and four Au/rGO/MnO_2 electrodes, respectively. The capacitance values calculated from the GCD curves in Figure 3E reveal an increase in capacitance from 1532 mF cm^{-2} (single device) to 3700 mF cm^{-2} (stacked device). Notably, previous studies have shown a linear increase in capacitance of parallel device configurations, depending upon the number of linked devices.[27,54,55] In the case here, the increase in capacitance of the stacked assembly is more than doubled compared to the single device (Figure 3E). The nonlinear increase in capacitance could be attributed to the lower mean ion-diffusion pathway enabled by the vertical stacking of the electrodes.[6,56] This result constitutes further evidence of the advantages in the Au/rGO/MnO_2 device architecture. Overall, the excellent electrochemical performance of the Au/rGO/MnO_2-based microsupercapacitors, outlined in Figure 3, demonstrates the potential of the electrodes as viable conduits for energy-storage applications.

Conclusions

A new high areal energy density microsupercapacitor comprising freestanding microporous gold/reduced graphene oxide/manganese oxide (Au/rGO/MnO_2) electrodes was constructed. The electrode was fabricated through a simple self-assembly synthetic route, producing a conductive Au/rGO framework serving both as scaffold for deposition of the pseudocapacitive MnO_2 layer as well as the current collector of the electrode thereby reducing the overall volume and weight of the electrode and devices. The nano-to-micro porous structure of the Au/rGO/MnO_2 electrodes provided an extensive surface area and enabled highly efficient diffusion of the electrolyte, as reflected in the superior electrochemical properties of the electrode, particularly low resistance and high areal capacitance at high current densities. Symmetric solid-state devices composed of two and four Au/rGO/MnO_2 electrodes were fabricated, exhibiting high areal energy densities. Notably, the intrinsic freestanding nature of the electrodes enables multielectrode stacking in parallel supercapacitor devices having small volumes and excellent energy-storage capabilities. A vertical parallel-stacked microsupercapacitor was constructed, exhibiting a nonlinear increase in capacitance ascribed to the decrease in the mean ion-diffusion pathway due to the interdigitated architecture of the stacked electrodes.

Experimental Section

Materials

$HAuCl_4 \cdot 3H_2O$ and KSCN were purchased from Sigma–Aldrich and used as received. Sodium nitrate, potassium permanganate, lithiumchloride, manganous acetate, lithium sulfate, and sodium sulfate were purchased from Alfa Aesar and used as received. Acetonitrile was purchase from Bio Lab Ltd (Jerusalem, Israel). Water used in the experiments was doubly purified by a Branstead D7382 water purification system (Branstead Thermolyne, Dubuque, IA), at 18.3 MΩ resistivity.

Synthesis of graphene oxide

GO was synthesized through modified Hummers method.[57] Briefly, graphite flakes (1 g) were added to a round-bottom flask contain-

ing H_2SO_4 (46 mL) cooled in an ice bath. The mixture was then stirred for 1 h to disperse the graphite. After shifting the flask to a water bath, $NaNO_3$ (1 g) and $KMnO_4$ (6 g) were successively added very slowly (within 15 minutes). The temperature of the water bath was increased to 40 °C and the reaction mixture was stirred for 3 h. Deionized water (50 mL) was slowly added to the reaction mixture, followed by H_2O_2 (5 mL). Stirring was continued for another 10 min. The reaction mixture was then centrifuged (5000 rpm, 20 min) to separate the precipitate. Centrifugation was repeated until the supernatant showed a neutral pH. The resultant brown-colored GO residue was immersed in liquid nitrogen and freeze-dried using a lyophilizer. The GO was stored at 4 °C.

Synthesis of $KAu(SCN)_4$ complex

$HAuCl_4$ solution (1 mL, 20 mg mL^{-1}) was mixed with KSCN solution (1 mL, 24 mg mL^{-1}), and centrifuged at 4000 g for 20 min. The resulting precipitate was separated and dried at ambient conditions.

Preparation of Au/rGO hybrid electrode

GO solution (15 mg mL^{-1}) in a mixture of water/acetonitrile (3:5 volume ratio) was sonicated for 1 h. The GO solution (160 μL) was mixed with $KAu(SCN)_4$ (23 mg) and sonicated, at an ice bath, until the solution became homogeneous. After the GO/$KAu(SCN)_4$ mixture was cooled it was deposited on a 0.5 cm × 2 cm glass and left to dry at 4 °C. After solvent evaporation the glass samples were exposed to air plasma for 10 min at a pressure of 0.7 mbar and power of 85 W. After plasma treatment, the samples were immersed in water and left to dry before treated again with air plasma. After the third plasma treatment, the samples were incubated in a chamber containing of hydrazine (0.5 mL) at 90 °C for overnight reduction of the GO.

Deposition of MnO_2 on Au/rGO hybrid electrode

Au/rGO electrode was immersed in a 0.5 M $Mn(CH_3COO)_2$ and 0.5 M Na_2SO_4 solution. The deposition was done using a three-electrode configuration where the Au/rGO electrode was the working electrode, platinum wire was used as counter electrode, and Ag/AgCl as reference electrode. The deposition of MnO_2 was done at pulsed rate of 10 s, in which the voltage was set to 3 and 0 V (for 10 s) at different deposition times, ranging from 4 to 16 min.

SEM

For SEM measurements, Au/rGO and Au/rGO/MnO_2 were grown as described above on glass substrates. The SEM images were recorded using a JSM-7400 SEM (JEOL LTD, Tokyo, Japan) at an acceleration voltage of 3 kV and working distance of 8 mm.

Symmetric pseudocapacitor device fabrication

LiCl electrolyte was prepared by dissolving of LiCl (2 g) and PVA (2 g) in water (10 mL) at 80 °C overnight. The Au/rGO/MnO_2 electrode was placed on a silver paste deposited on polydimethylsiloxane (PDMS) stamp (Figure S9). A filter paper soaked with the LiCl electrolyte was then placed on the Au/rGO/MnO_2 electrode and finally another Au/rGO/MnO_2 electrode was placed on the filter paper. The electrolyte (80 μL) was drop-casted on the device and left to dry for 2 hours. The layer of PDMS was cast on the device and dried for 2 hours at 80 °C.

Electrochemical characterization

For CV and galvanostatic measurements a three-electrode configuration was used. Au/rGO electrode or Au/rGO/MnO_2 electrode was used as the working electrode, platinum wire as counter electrode, and Ag/AgCl as reference. The measurements were conducted in a 1 M LiCl solution at different scan rates and current densities. Device performance was evaluated in a two-electrode configuration. Experiments were conducted on a BioLogic SP-200 instrument.

Acknowledgements

We are grateful to the Ministry of Science and Technology (Kamin Program) and to the Israel Science Foundation (Grant 2014-14) for generous financial support. We thank Dimitry Mogiliansky for helping with the XRD experiments, Leila Zeiri for helping with Raman measurements, and Natalya Froumin for assistance with XPS measurements.

Conflict of interest

The authors declare no conflict of interest.

Keywords: graphene oxide · manganese oxide · microsupercapacitors · porous gold · pseudocapacitance

[1] P. Yang, W. Mai, *Nano Energy* **2014**, *8*, 274 – 290.
[2] M. Yu, W. Qiu, F. Wang, T. Zhai, P. Fang, X. Lu, Y. Tong, *J. Mater. Chem. A* **2015**, *3*, 15792 – 15823.
[3] P. Simon, Y. Gogotsi, *Nat. Mater.* **2008**, *7*, 845 – 854.
[4] W. Deng, X. Ji, Q. Chen, C. E. Banks, *RSC Adv.* **2011**, *1*, 1171.
[5] S. Chu, Y. Cui, N. Liu, *Nat. Mater.* **2016**, *16*, 16 – 22.
[6] M. Beidaghi, Y. Gogotsi, *Energy Environ. Sci.* **2014**, *7*, 867.
[7] A. S. Aricò, P. Bruce, B. Scrosati, J.-M. Tarascon, W. van Schalkwijk, *Nat. Mater.* **2005**, *4*, 366 – 377.
[8] G. Yu, X. Xie, L. Pan, Z. Bao, Y. Cui, *Nano Energy* **2013**, *2*, 213 – 234.
[9] F. Yao, D. T. Pham, Y. H. Lee, *ChemSusChem* **2015**, *8*, 2284 – 2311.
[10] J. B. Goodenough, Y. Kim, *Chem. Mater.* **2010**, *22*, 587 – 603.
[11] M. Winter, R. J. Brodd, *Chem. Rev.* **2004**, *104*, 4245 – 4269.
[12] J. Jiang, Y. Li, J. Liu, X. Huang, C. Yuan, X. W. D. Lou, *Adv. Mater.* **2012**, *24*, 5166 – 5180.
[13] B. E. Conway, *J. Electrochem. Soc.* **1991**, *138*, 1539.
[14] Y. Zhang, H. Feng, X. Wu, L. Wang, A. Zhang, T. Xia, H. Dong, X. Li, L. Zhang, *Int. J. Hydrogen Energy* **2009**, *34*, 4889 – 4899.
[15] B. E. Conway, W. G. Pell, *J. Solid State Electrochem.* **2003**, *7*, 637 – 644.
[16] V. Augustyn, P. Simon, B. Dunn, *Energy Environ. Sci.* **2014**, *7*, 1597.
[17] L. Y. Chen, Y. Hou, J. L. Kang, A. Hirata, T. Fujita, M. W. Chen, *Adv. Energy Mater.* **2013**, *3*, 851 – 856.
[18] X. Lang, A. Hirata, T. Fujita, M. Chen, *Nat. Nanotechnol.* **2011**, *6*, 232 – 236.
[19] C. Choi, H. J. Sim, G. M. Spinks, X. Lepró, R. H. Baughman, S. J. Kim, *Adv. Energy Mater.* **2016**, *6*, 1502119.
[20] Y. Zhao, L. Hu, S. Zhao, L. Wu, *Adv. Funct. Mater.* **2016**, *26*, 4085 – 4093.
[21] C. Hao, B. Yang, F. Wen, J. Xiang, L. Li, W. Wang, Z. Zeng, B. Xu, Z. Zhao, Z. Liu, Y. Tian, *Adv. Mater.* **2016**, *28*, 3194 – 3201.
[22] Q. Meng, H. Wu, Y. Meng, K. Xie, Z. Wei, Z. Guo, *Adv. Mater.* **2014**, *26*, 4100 – 4106.
[23] G. Yu, L. Hu, N. Liu, H. Wang, M. Vosgueritchian, Y. Yang, Y. Cui, Z. Bao, *Nano Lett.* **2011**, *11*, 4438 – 4442.
[24] R. Amade, E. Jover, B. Caglar, T. Mutlu, E. Bertran, *J. Power Sources* **2011**, *196*, 5779 – 5783.
[25] Y. Chen, L. Du, P. Yang, P. Sun, X. Yu, W. Mai, *J. Power Sources* **2015**, *287*, 68 – 74.

[26] Z. J. Han, Z. Bo, D. H. Seo, S. Pineda, Y. Wang, H. Y. Yang, K. K. Ostrikov, *ChemSusChem* **2016**, *9*, 1020 – 1026.
[27] L. Li, J. Zhang, Z. Peng, Y. Li, C. Gao, Y. Ji, R. Ye, N. D. Kim, Q. Zhong, Y. Yang, H. Fei, G. Ruan, J. M. Tour, *Adv. Mater.* **2016**, *28*, 838 – 845.
[28] A. Ferris, S. Garbarino, D. Guay, D. Pech, *Adv. Mater.* **2015**, *27*, 6625 – 6629.
[29] L. Zhang, P. Zhu, F. Zhou, W. Zeng, H. Su, G. Li, J. Gao, R. Sun, C. Wong, *ACS Nano* **2016**, *10*, 1273 – 1282.
[30] S. S. Patil, D. P. Dubal, M. S. Tamboli, J. D. Ambekar, S. S. Kolekar, P. Gomez-Romero, B. B. Kale, D. R. Patil, *J. Mater. Chem. A* **2016**, *4*, 7580 – 7584.
[31] A. Morag, T. Golub, J. Becker, R. Jelinek, *J. Colloid Interface Sci.* **2016**, *472*, 84 – 89.
[32] A. Morag, V. Ezersky, N. Froumin, D. Mogiliansky, R. Jelinek, *Chem. Commun.* **2013**, *49*, 8552.
[33] T. M. Higgins, D. McAteer, J. C. M. Coelho, B. M. Sanchez, Z. Gholamvand, G. Moriarty, N. McEvoy, N. C. Berner, G. S. Duesberg, V. Nicolosi, J. N. Coleman, *ACS Nano* **2014**, *8*, 9567 – 9579.
[34] R. Wang, X. Yan, *Sci. Rep.* **2014**, *4*, 3712.
[35] Y. Yesi, I. Shown, A. Ganguly, T. T. Ngo, L.-C. Chen, K.-H. Chen, *ChemSusChem* **2016**, *9*, 370 – 378.
[36] Y. Xu, Z. Lin, X. Huang, Y. Wang, Y. Huang, X. Duan, *Adv. Mater.* **2013**, *25*, 5779 – 5784.
[37] Y. Xu, Z. Lin, X. Huang, Y. Liu, Y. Huang, X. Duan, *ACS Nano* **2013**, *7*, 4042 – 4049.
[38] L. B. Thompson, N. H. Mack, R. G. Nuzzo, *Phys. Chem. Chem. Phys.* **2010**, *12*, 4301 – 4308.
[39] M. Beidaghi, C. Wang, *Adv. Funct. Mater.* **2012**, *22*, 4501 – 4510.
[40] W. H. Qu, Y. B. Guo, W. Z. Shen, W. C. Li, *J. Phys. Chem. C* **2016**, *120*, 15105 – 15113.
[41] K. Sheng, Y. Sun, C. Li, W. Yuan, G. Shi, *Sci. Rep.* **2012**, *2*, 247.
[42] L. Zhang, C. Yang, N. Hu, Z. Yang, H. Wei, C. Chen, L. Wei, Z. J. Xu, Y. Zhang, *Nano Energy* **2016**, *26*, 668 – 676.
[43] K. Shi, X. Yang, E. D. Cranston, I. Zhitomirsky, *Adv. Funct. Mater.* **2016**, *26*, 6437 – 6445.
[44] T. M. Dinh, A. Achour, S. Vizireanu, G. Dinescu, L. Nistor, K. Armstrong, D. Guay, D. Pech, *Nano Energy* **2014**, *10*, 288 – 294.
[45] P. Sheng, W. Li, X. Tong, X. Wang, Q. Cai, *J. Mater. Chem. A* **2014**, *2*, 18974 – 18987.
[46] M. Nasibi, M. A. Golozar, G. Rashed, *Mater. Lett.* **2013**, *91*, 323 – 325.
[47] S. F. Shaikh, J. Y. Lim, O.-S. Joo, *Curr. Appl. Phys.* **2013**, *13*, 758 – 761.
[48] K. Vijaya Sankar, S. Surendran, K. Pandi, A. M. Allin, V. D. Nithya, Y. S. Lee, R. Kalai Selvan, *RSC Adv.* **2015**, *5*, 27649 – 27656.
[49] T. Qin, B. Liu, Y. Wen, Z. Wang, X. Jiang, Z. Wan, S. Peng, G. Cao, D. He, *J. Mater. Chem. A* **2016**, *4*, 9196 – 9203.
[50] Z. Fan, J. Yan, T. Wei, L. Zhi, G. Ning, T. Li, F. Wei, *Adv. Funct. Mater.* **2011**, *21*, 2366 – 2375.
[51] W. Liu, X. Yan, J. Lang, C. Peng, Q. Xue, *J. Mater. Chem.* **2012**, *22*, 17245.
[52] W.-C. Chen, T.-C. Wen, H. Teng, *Electrochim. Acta* **2003**, *48*, 641 – 649.
[53] Y. Wang, Z. Shi, Y. Huang, Y. Ma, C. Wang, M. Chen, Y. Chen, *J. Phys. Chem. C* **2009**, *113*, 13103 – 13107.
[54] M. F. El-Kady, R. B. Kaner, *Nat. Commun.* **2013**, *4*, 1475.
[55] H. Zhang, H. Su, L. Zhang, B. Zhang, F. Chun, X. Chu, W. He, W. Yang, *J. Power Sources* **2016**, *331*, 332 – 339.
[56] D. Pech, M. Brunet, H. Durou, P. Huang, V. Mochalin, Y. Gogotsi, P.-L. Taberna, P. Simon, *Nat. Nanotechnol.* **2010**, *5*, 651 – 654.
[57] S. Hummers, R. E. Offeman, *J. Am. Chem. Soc.* **1958**, *80*, 1339.

Manuscript received: March 23, 2017
Revised manuscript received: May 4, 2017
Accepted manuscript online: May 5, 2017
Version of record online: May 24, 2017